







A 1 bit Raw Voltage-recording System for Dedicated Observations of Transients at Low Radio Frequencies

Kshitij S. Bane¹ , Indrajit V. Barve², G. V. S. Gireesh² , C. Kathiravan¹ , and R. Ramesh¹ ¹Indian Institute of Astrophysics, Koramangala 2nd Block, Bangalore 560034, Karnataka, India
²Radio Astronomy Field Station, Indian Institute of Astrophysics, Gauribidanur 561210, Karnataka, India
Received 2023 December 31; revised 2024 April 13; accepted 2024 April 22; published 2024 May 16

Abstract

Recently we had reported commissioning of a prototype for pulsar observations at low radio frequencies (<100 MHz) using log-periodic dipole antennas in the Gauribidanur Radio Observatory ($\approx 77^\circ\text{E}$, 14°N) near Bangalore in India (<https://www.iiap.res.in/?q=centers/radio>). The aforementioned system (the Gauribidanur Pulsar System) is currently being augmented to directly digitize the radio-frequency signals from the individual antennas in the array. Our initial results using a 1 bit raw voltage-recording system indicate that such a back-end receiver offers distinct advantages like (i) simultaneous observations of any set of desired directions in the sky with multiple offline beams and smaller data rate/volume, and (ii) archival of the observed data with minimal resources for reanalysis in the future, either in the same or a different set of directions in the sky.

Unified Astronomy Thesaurus concepts: [Astronomical instrumentation \(799\)](#); [Radio astronomy \(1338\)](#); [Pulsars \(1306\)](#)

1. Introduction

The latest advancements in commercial technology help to directly digitize the radio-frequency (RF) signals in radio astronomy observations and record them as sampled voltages. Traditionally, a receiver architecture includes one or several mixer stages performing downconversion from RF to an intermediate or baseband frequency, due to a limited analog-to-digital (ADC) sampling rate. However, in pace with technology development, increased ADC performance allows for higher sampling rates. The higher the sampling rate, the higher the frequency that can be sampled for a correct read, thereby allowing sampling at either the observation frequency itself or a higher intermediate frequency. Accordingly, at a sufficiently high sample rate there would be no need for downconversion. Eliminating the need for a mixer stage is advantageous, since mixers in practice raise system challenges, such as introducing frequency offsets. In addition to minimizing the number of analog components in the receiver system and thereby the associated amplitude/phase variations, the direct digitization offers more flexibility, particularly in the efforts to search for radio transients at low frequencies where the individual dipole antennas have wider instantaneous sky coverage. For example, in the multibeam setup where beams are formed on board digital hardware like a field-programmable gate array (FPGA), the number of beams is limited by the resources available on the FPGA. Also, once the beams are formed in certain directions, the observations are limited to the corresponding directions. On the contrary, if raw voltages from each antenna are recorded, any number of beams can be formed offline to probe any desired set of directions in the sky within the field of view of the individual antenna. Therefore, it is advantageous to have a voltage-recording capability. A high sampling rate and high-resolution ADC accordingly approach an accurate read of

an incoming signal, which is seemingly preferable. However, the energy consumption at high sampling frequencies increases with the number of quantization levels.³ Furthermore, the resulting data volumes and subsequent data processing/management will be enormous in such a system. One solution to these is to record a fewer number of bits from ADCs connected to each antenna element. Data rates and volumes can be significantly reduced if 1 bit (sign bit) digital receivers are employed. 1 bit digital correlators have been used in radio astronomy (see e.g., Weinreb 1963; Udaya Shankar & Ravi Shankar 1990; Nakajima et al. 1994; Ebenezer et al. 2001; Ramesh et al. 2008; Zakharenko et al. 2016). The present work describes a 1 bit raw voltage capture system that we have implemented in the Gauribidanur Pulsar System (GAPS) to demonstrate how such a system could be useful for observations of pulsars and other transients at low radio frequencies.

2. The Antenna and Analog Receiver System

GAPS is a recently commissioned prototype using log-periodic dipole antennas (LPDAs) for observations of the transients in the frequency range $\approx 35\text{--}85$ MHz. The antenna array has 16 LPDAs arranged on a north–south baseline with spacing of 5 m between the adjacent antennas (Bane et al. 2022). For the present work, we used only eight LPDAs (see Figure 1). The half-power beamwidth (HPBW) of each LPDA in the GAPS is $\approx 80^\circ$ in the E-plane where the arms of the LPDA are present, and $\approx 110^\circ$ in the orthogonal H-plane. All the LPDAs have been mounted with their H-plane in the east–west direction and E-plane in the north–south direction. The effective collecting area and gain of each LPDA is $\approx 0.4\lambda^2$ (where λ is the wavelength corresponding to the observing frequency) and ≈ 6.5 dBi (with respect to an isotropic radiator), respectively. The characteristic impedance of the LPDA is $\approx 50\ \Omega$. The voltage standing wave ratio (VSWR) is < 2 over the frequency range $\approx 40\text{--}440$ MHz. Since the LPDAs are arranged on a north–south baseline, the combined response

³ <https://github.com/bmurrmann/ADC-survey>

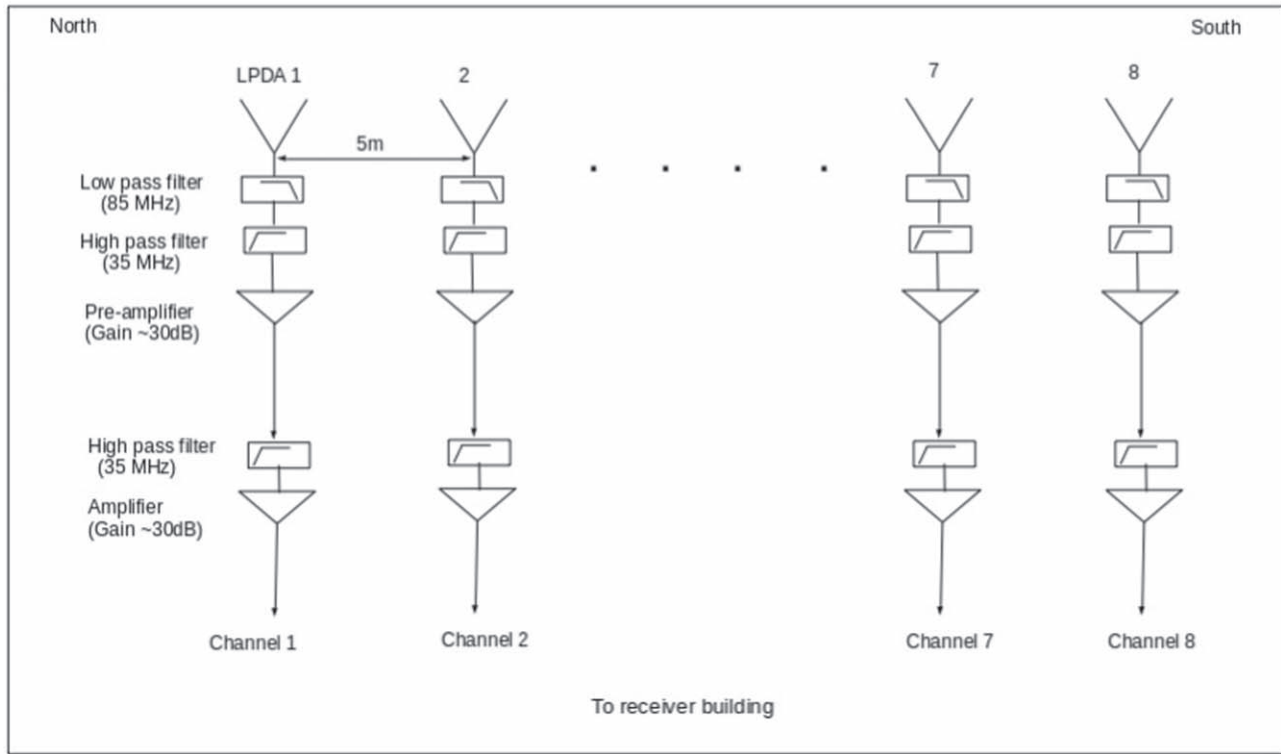


Figure 1. GAPS array configuration used in the present work.

pattern of the array (eight LPDAs) after coherent beam formation is $\approx 110^\circ$ in the east–west (hour angle/R.A.) direction and $\approx 6^\circ$ in the north–south (decl.) direction for observations near the zenith at a typical frequency like 60 MHz. It is a fan beam with the above resolution in decl. The width of the east–west response pattern is nearly independent of frequency. Being very wide, it helps to observe a radio source continuously for ≈ 7 hr. This is useful since mechanical steering is difficult for the dipole antennas used at low frequencies (see e.g., Ramesh et al. 1999, 2012). An LMR-200 coaxial cable⁴ connected to the feedpoint near the top of the LPDA transmits the RF signal incident on the LPDA to the input of a low-pass filter with 3 dB cutoff at ≈ 85 MHz followed by a high-pass filter with 3 dB cutoff at ≈ 35 MHz, and then a wideband amplifier with an uniform gain ≈ 30 dB in the frequency range 35–85 MHz. The two filters and the amplifier are kept near the base of the LPDA to minimize the length of the LMR-200 cable and hence the transmission loss. The high- and low-pass filters help to attenuate the unwanted signal at frequencies $\lesssim 30$ MHz and $\gtrsim 85$ MHz. Both the filters have a steep reduction in gain beyond their cutoff frequencies. For example, the amplitude of the input signal is reduced by ≈ 30 dB at 25 MHz and 95 MHz in the aforementioned high- and low-pass filters, respectively. Due to this, amplification of any RF interference (RFI) present outside the frequency range of our observation (i.e., 35–85 MHz) is very minimal. The passband is relatively free of RFI (see e.g., Bane et al. 2022). The outputs corresponding to each LPDA are then transmitted to a central cabin near the center of the array where they are again high-pass filtered and amplified. Note that the second high-pass filter in the signal chain further suppresses the RFI at

frequencies $\lesssim 30$ MHz. The RF signals are then transferred to the receiver building (located ≈ 300 m away) independently via eight separate, low-loss LMR-400 coaxial cables⁵ of identical RF characteristics. The lengths of all the cables are the same and they were also phase equalized. The cables are buried ≈ 1 m below the ground level to minimize possible diurnal variations in their characteristics.

The array was initially equipped with an analog beamformer network (Bane et al. 2022) where phase/delay cables controlled by diode switches were used to observe a particular direction of the sky at any given epoch (see, e.g., Landecker 1984; Ramesh et al. 1998). Different lengths of phase/delay cables must be used in the latter to observe different regions of the sky. This introduces systematic gain variations. Furthermore, simultaneous observations are practically difficult. Once the beam is formed in a particular direction, observations will be restricted to that direction. These are common to any other similar analog hardware used elsewhere. Note that we used only eight LPDAs in the GAPS for the present work since our aim is to understand the digital beamformer described in the present work for future use with the Gauribidanur RADioheliograPH (GRAPH), which has eight LPDAs per group (Ramesh 2011; Ramesh et al. 2014), and use GRAPH for dedicated observations of nonsolar transients, particularly during the local nighttime. Further, the ADCs available to us can also only handle eight inputs. Note that the GRAPH is a T-shaped radio interferometer array consisting of 512 LPDAs. The individual arms of the array are oriented along the east–west and south directions. The effective collecting area (A_e) of the array is ≈ 6400 m² at a typical frequency like 60 MHz. The sky coverage is ≈ 8800 square

⁴ <https://timesmicrowave.com/wp-content/uploads/2022/06/lmr-200-datasheet.pdf>

⁵ <https://timesmicrowave.com/wp-content/uploads/2022/06/lmr-400-datasheet.pdf>

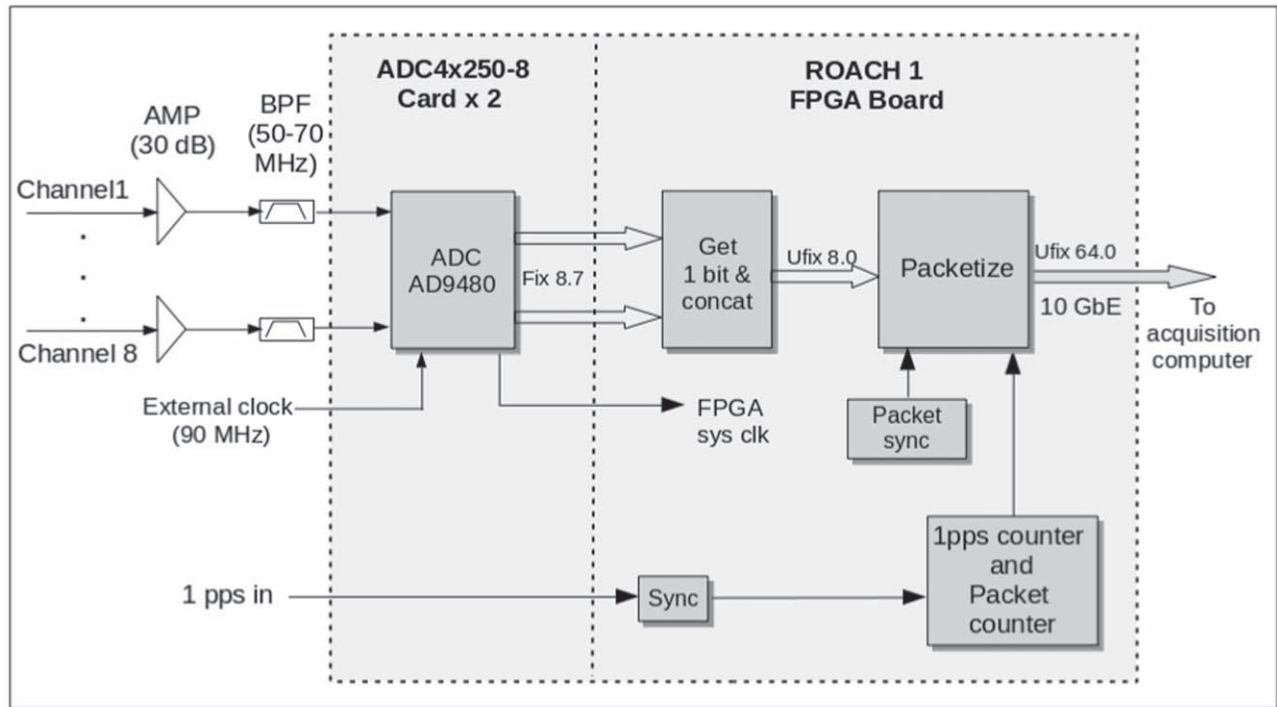


Figure 2. The 1 bit raw voltage-recording system used in the GAPS.

degrees, independent of frequency. Both these numbers are reasonably large, an important requisite for observations of nonsolar transients. For comparison, the fully completed NenuFAR in France is expected to have $A_e \approx 20,000 \text{ m}^2$ and sky coverage ≈ 100 square degrees, at 60 MHz.⁶ The corresponding numbers for LOFAR, which is currently operational, are $A_e \approx 9600 \text{ m}^2$ and sky coverage $\approx 19,600$ square degrees, at 60 MHz (van Haarlem et al. 2013). The aforementioned characteristics of GRAPH, along with the prospects of a dedicated and continuous observing period of ≈ 14 hr every day exclusively for nonsolar transients, suggests that GRAPH could be an useful instrument.

3. The Digital Receiver System

Figure 2 shows the schematic of the 1 bit raw voltage-recording receiver. The digital receiver is implemented on Reconfigurable Open Architecture Computing Hardware (ROACH) from the Collaboration for Astronomy Signal Processing and Electronics Research. The ROACH board hardware has the Xilinx Virtex-5 FPGA.⁷ The RF signals from the each of the eight antennas pass through an independent amplifier and bandpass filter of 50–70 MHz before being fed to ADCs. We have used two quad-ADC cards, each containing four AD9480 integrated circuits.⁸ The signals are sampled at 90 MHz. A single clock is used to sample all the antennas. The sampled band lies in the second Nyquist zone of 90 MHz. The ADC converts the input voltage to an 8 bit fixed-point number (Fix 8.7) between -1 and $+1$. The sign bit from each of these numbers is separated. So, we have 1 bit from each antenna channel. Therefore, the ADC output is an unsigned 8 bit number (UFix8.0) representing the input voltage from each of

the eight channels. Such 1024×8 8 bit numbers are packeted together and sent to the recording computer over 10 Gbit Ethernet (10GbE). Note that 10GbE allows transmission of 64 bit numbers.⁹ So, one packet has 1024 64 bit numbers. This results in a data rate of $\approx 0.72 \text{ Gbit s}^{-1}$. This is much smaller compared to the the data rate of $\approx 5.6 \text{ Gbit s}^{-1}$ which would have resulted if 8 bits were recorded from each antenna channel. To avoid packet losses while recording, the data is captured using the n2disk program¹⁰ on a 32 GB RAM computer. Each packet also contains a user datagram protocol header (58 bytes) and a custom header (80 bytes) that contain the observation details, 1 pulse per second (PPS) count, and a packet count. The 1 PPS signal is derived from a GPS clock¹¹ and given to the FPGA via the ADC card to generate the 1 PPS count. The packet count is a unique packet number assigned to each packet. It is used to check for any packet losses. The recorded file contains a time series of 1 bit voltages from each antenna channel. Some of the characteristics are listed in Table 1.

4. Offline Beam Formation

Figure 3 shows the offline beam-forming pipeline. First, the packets are unscrambled to get voltage time series of the individual antenna channels. Delays are applied to these time series according to the desired decl. where the beam needs to be formed. Note that the array is oriented in the north–south direction, so the beam formation is performed along the decl. Based on the decl., the geometric delays are calculated using the formula $t_j = d_j \sin \theta / c$, where t_j is the delay required for the

⁶ <https://nenufar.obs-nancay.fr/en/astromer/>

⁷ <https://casper.astro.berkeley.edu/wiki/ROACH>

⁸ <https://www.analog.com/en/products/AD9480.html>

⁹ https://casper-toolflow.readthedocs.io/projects/tutorials/en/latest/tutorials/roach/tut_ten_gbe.html

¹⁰ <https://www.ntop.org/products/traffic-recording-replay/n2disk/>

¹¹ <https://novotech.com/wp-content/uploads/2022/11/Thunderbolt-E-GPS-Disciplined-Clock-Data-Sheet.pdf>

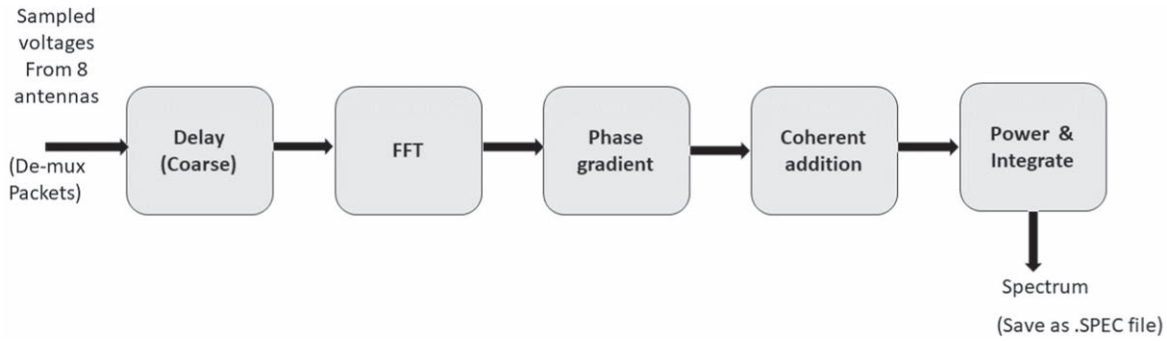


Figure 3. Offline beam-forming pipeline used in the GAPS.

Table 1
Characteristics of GAPS

Parameter	Value
Number of channels	8
Sampling rate	90 MSPS
Sampled bits	1
Observation band	45–90 MHz (50–70 MHz for the present work)
Beam formation	Offline
FFT size	Variable (8192 for the present work)
Frequency resolution	10.98 kHz
Postdetection time resolution	Variable (minimum 91.02 μ s for one spectrum)
Decl. coverage	-26.4° S to $+53.6^\circ$ N

j th antenna at a distance of d_j from the reference antenna for the source at angle θ , and c is the speed of light. The sampling interval (t_s) is $1/90$ MHz = 11.11 ns. So, the time series are delayed by the closest integer multiple of 11.11 ns (i.e., mt_s , where m is an integer). The uncompensated fractional delays ($\Delta t_j = t_j - mt_s$) can be compensated by applying a phase gradient in the spectral domain, i.e., $\phi_{j,k} = 2\pi F_k \Delta t_j$, where F_k is the k th frequency bin. The delayed voltage streams are Fourier transformed using a fast Fourier transform (FFT). Subsequently, the phase compensation is performed by multiplying the complex Fourier output by $e^{-i\phi_j}$. An 8192-point FFT is performed, resulting in 4096 positive frequency bins with a resolution of 10.986 kHz. The number of FFT points and hence the resolution can be changed depending on the requirement, since the beam formation is performed offline. After the phase compensation, the individual spectra from each antenna are added together, modulo-squared, and integrated according to the desired temporal resolution. Multiple beams pointing at different decl. can be formed by changing the delay and phase values. A “.SPEC” file is stored for each beam containing the corresponding power-spectrum series. These are further processed using the standard Pulsar Exploration and Search Toolkit (PRESTO; Ransom 2011).

5. Observations

The initial run of the new system was carried out on 2023 August 10 for ≈ 5 hr, starting from $\approx 08:49$ local sidereal time (LST). Three beams pointing toward declinations 6.17° N, 7.92° N, and 15.85° N were formed offline from the raw voltage data recorded. The power-spectrum series from these three beams were stored in three separate .SPEC files with time

resolutions of 4 ms, 2 ms and 1 ms, respectively. The files were converted to SIGPROC “filterbank” (.fil) format.¹² As first step, RFI excision was performed using *rficlean* (Maan et al. 2021) to mitigate strong periodic RFI. Subsequently we used *rfifind* from PRESTO, which searches for time and frequency domain RFI and creates mask files. This is followed by *prepfold* which is used to fold and dedisperse the data and detect pulsars. Three pulsars B0834+06 (J0837+0610), B0950+08 (J0953+0755), and B1133+16 (J1136+1551) were detected in the above three beams, respectively (see Figures 4 and 5). A solar event (type III burst, McLean & Labrum 1985; Ramesh & Ebenezer 2001) was also recorded during the observation at $\approx 11:03$ LST. The decl. of the Sun was $\approx 15.7^\circ$ N. A separate beam was formed pointing toward the above decl. with a time resolution of ≈ 10 ms. We carried out analysis with a single-pulse search pipeline developed using PRESTO routines. The maximum signal-to-noise ratio (S/N) was obtained for a dispersion measure (DM) ≈ 13.2 pc cm⁻³. The dedispersed dynamic spectrum of the solar burst is shown in Figure 6. The burst was also noticed in the observations carried out with the solar radio spectrographs in the Gauribidanur observatory (Benz et al. 2009; Kishore et al. 2014).

To verify the performance of GAPS, we formed 41 beams covering the decl. range from -26.3° S to $+53.7^\circ$ N in steps of 2° for the duration of the solar burst in Figure 6. The mean count during the solar burst at 60 MHz in each of the 41 beams were obtained. The count is highest for the beam closest to the Sun’s decl. A Gaussian fit to the data points indicates HPBW $\approx 6^\circ$ (see Figure 7), which matches with the predicted HPBW of the GAPS antenna array in the present case (see Section 2). On 2023 October 18, a 4 hr observation run starting at $\approx 17:27$ LST was carried out. A beam was formed pointing toward decl. $\approx 21.88^\circ$ N with 4 ms time resolution. Pulsar B1919+21 (J1921+2153) was detected in this data (see Figure 5). A subsequent observation for a period of ≈ 7.2 hr was performed on 2023 October 21 starting at $\approx 06:36$ LST. Pulsars B0834+06 (J0837+0610), B0919+06 (J0922+0638), B0950+08 (J0953+0755), B0943+10 (J0946+0951), and B1133+16 (J1136+1551) were detected using ≈ 6 hr data around the transit of each pulsar (see Figure 5). Four beams were formed pointing toward declinations 6.17° N, 7.92° N, 9.86° N, and 15.85° N with 1 ms resolution. Pulsars B0834+06 and B0919+06 were detected in the same beam. The estimated parameters of the different pulsars mentioned above are listed in Table 2. The

¹² <http://sigproc.sourceforge.net/sigproc.pdf>

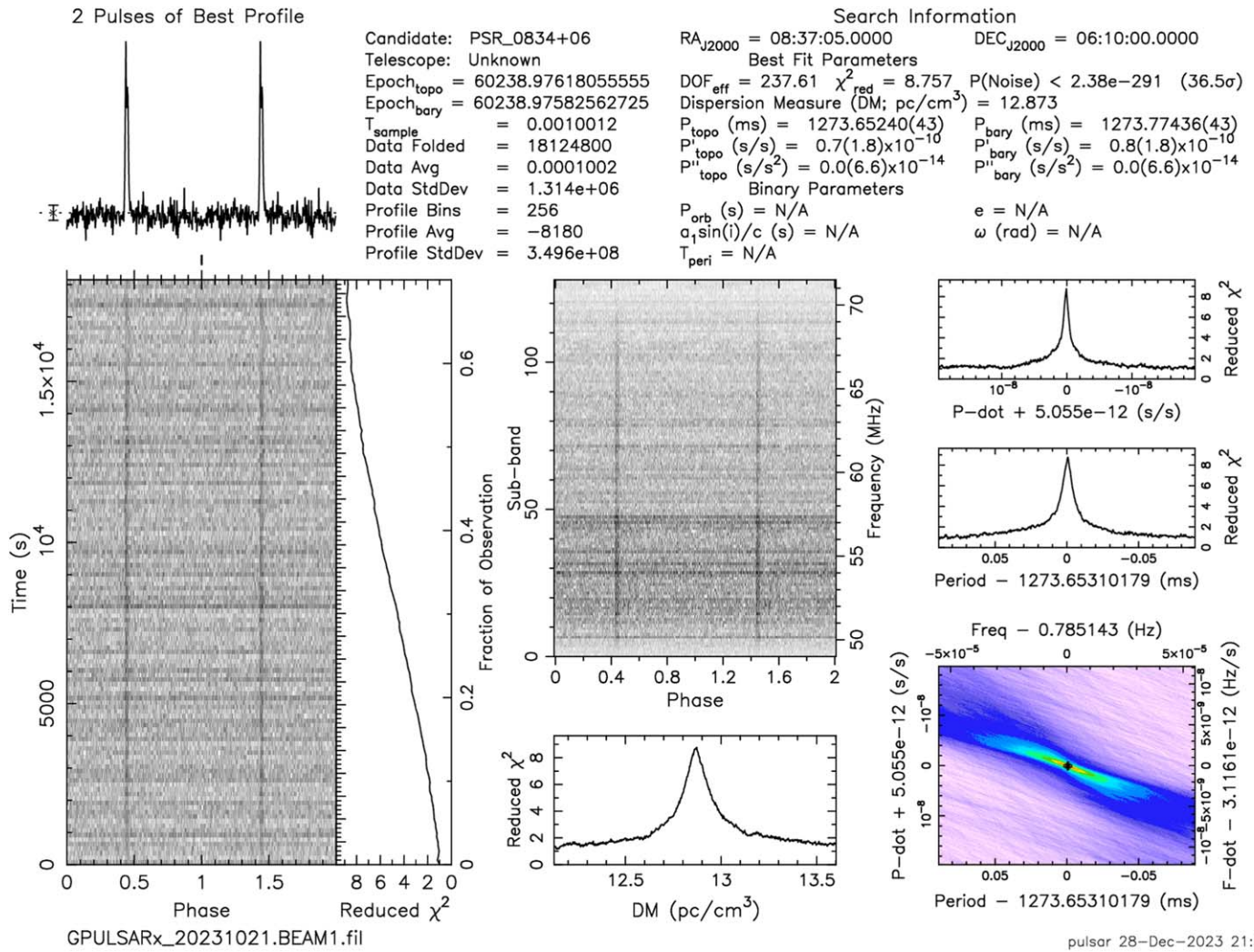


Figure 4. Observations of the pulsar B0834+06 (J0837+0610) on 2023 October 21 with GAPS in the frequency range of 50–70 MHz for a period of \approx 4 hr. The data were analyzed using PRESTO.

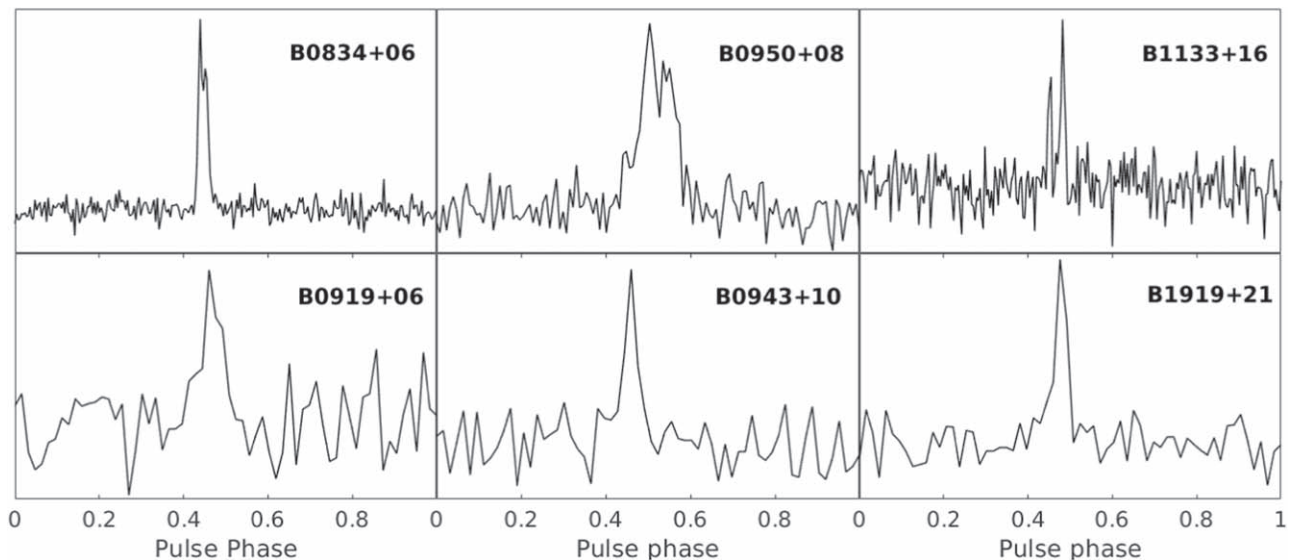


Figure 5. Average profiles of the pulsars observed with GAPS using a 1 bit raw voltage-recording system and offline beam formation.

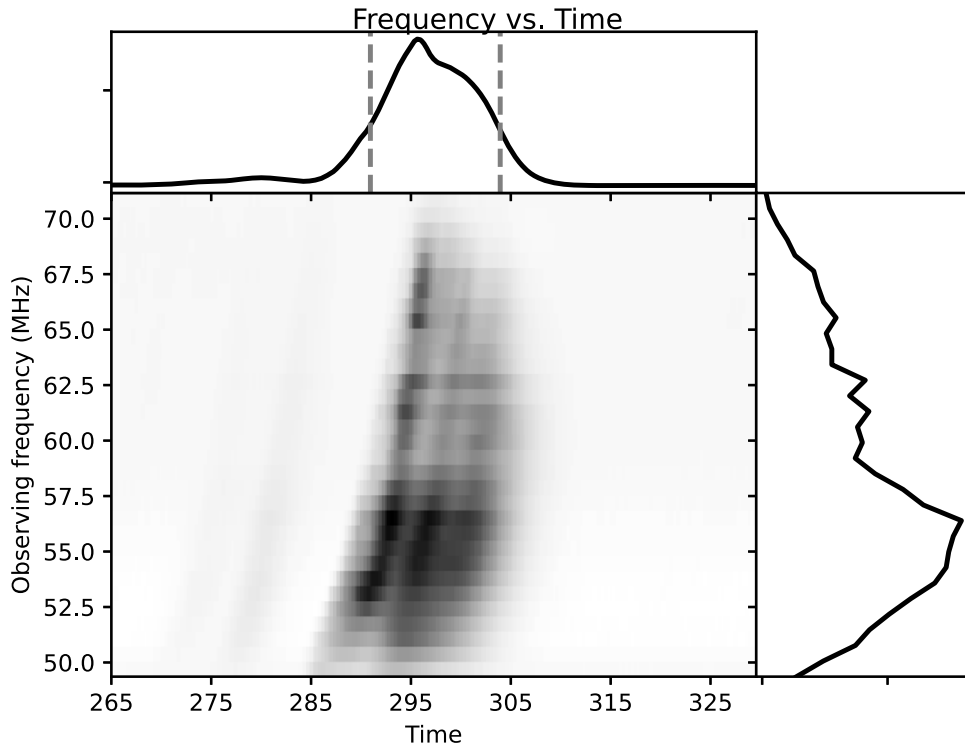


Figure 6. A dedispersed dynamic spectrum (50–70 MHz) corresponding to the type III solar radio burst observed with GAPS on 2023 August 10. The DM used was $\approx 13.2 \text{ pc cm}^{-3}$. The time in the x -axis starts from $\approx 11:02:30$ LST, and the interval is 10 s. The upper panel shows the spectrally averaged time profile of the burst. The right panel shows the temporally averaged spectral profile of the burst. The dotted lines in the upper panel indicate the main phase of the burst.

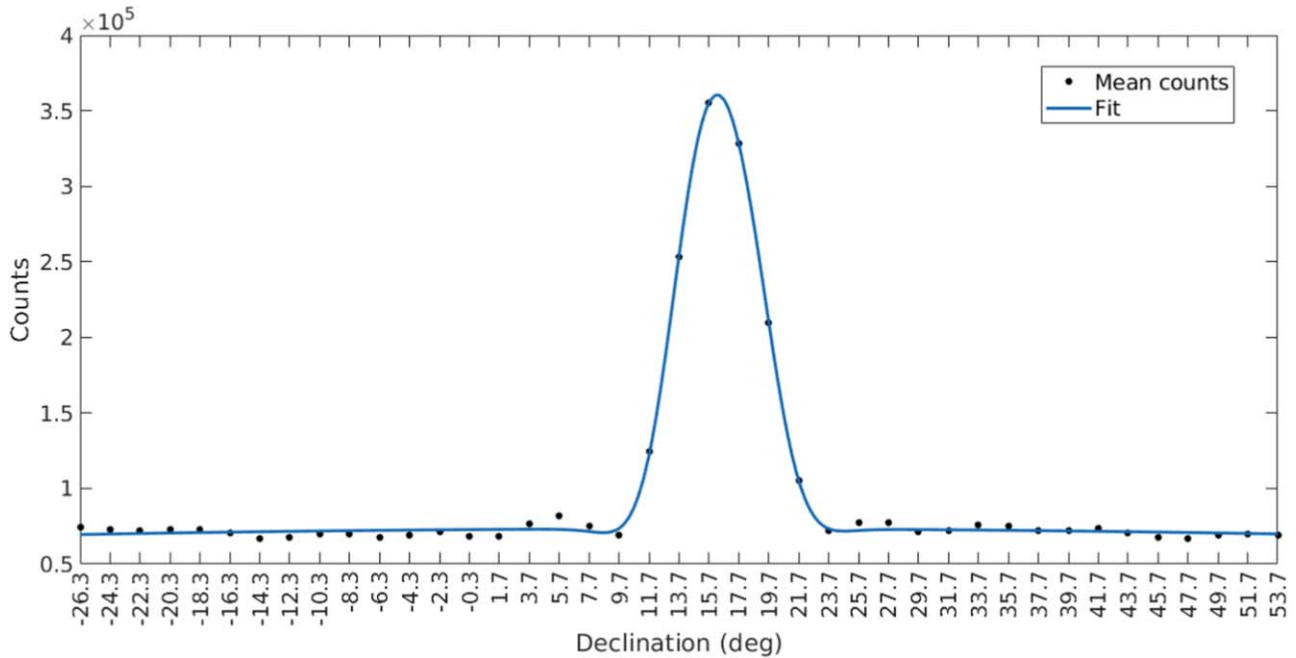


Figure 7. The decl. beam of GAPS at 60 MHz obtained by using multiple beams formed during the solar observations in Figure 6.

corresponding numbers reported previously by Bondonneau et al. (2020) from online, multibit digitization observations elsewhere in nearly the same frequency range are mentioned within the brackets. The period and DM for each pulsar in the two cases agree well. The pulsar average profiles in Figure 5 also closely match with the average profiles at low frequencies reported in the literature (Malov & Malofeev 2010; Hassall et al. 2012; Zakharenko et al. 2013; Stovall et al. 2015; Pilia

et al. 2016; Bilous et al. 2020; Bondonneau et al. 2020). Any minor differences are likely due to noisy detections in the present case. For example in the case of Bondonneau et al. (2020), the bandwidth and A_e used were higher than the present observations by factors of ≈ 2.75 and ≈ 10 , respectively. Furthermore, 12 bit ADC was used in their observations. Its quantization efficiency is $\approx (1/0.64)$ times higher than that of the 1 bit ADC used in the present observations (Thompson

Table 2
Characteristics of the Pulsars Observed with GAPS Using a 1 bit Raw Voltage-recording System

Pulsar	Period (s)	DM (pc cm ⁻³)	Duty Cycle (%)	S/N (folded)	Observing Duration (hr)
B0834+06	1.274 ± 0.000043 (1.274)	12.873 ± 0.05 (12.864)	6.4 ± 0.8 (6.9)	36.5 (309)	6 (1)
B0919+06	0.431 ± 0.000016 (0.431)	27.330 ± 0.02 (27.296)	14.4 ± 0.8 (15.4)	6.0 (144)	6 (3)
B0943+10	1.098 ± 0.000069 (1.098)	15.348 ± 0.02 (15.329)	12.9 ± 0.8 (15.2)	6.3 (148)	6 (2.5)
B0950+08	0.253 ± 0.000050 (0.253)	2.965 ± 0.05 (2.971)	15.3 ± 0.8 (14.6)	24.6 (140)	6 (1)
B1133+16	1.188 ± 0.000023 (1.188)	4.848 ± 0.03 (4.846)	12.7 ± 0.8 (18.7)	8.4 (261)	6 (2)
B1919+21	1.337 ± 0.000017 (1.337)	12.420 ± 0.02 (12.437)	7.8 ± 0.8 (8.4)	12.5 (180)	4 (1)

Note. Numbers within the brackets are from Bondonneau et al. (2020).

et al. 2001). The duration of observation for the respective pulsars in the two cases are also different. If we all these factors take into consideration, then the expected S/N for the pulsar B0834+06 in GAPS observations as compared to Bondonneau et al. (2020) is $\frac{309 * 0.64}{10\sqrt{2.75/6}} \approx 30$. Compared to this, the observed S/N with GAPS is ≈ 36 . Note that the duty cycle mentioned in Table 1 corresponds to the effective pulse width in pulse profiles at 50% of the highest peak intensity (i.e., w50).

6. Conclusions





We have presented a 1 bit raw voltage-recording system for observations of pulsars at low RFs. Other than reduction in the sensitivity, which could partly be compensated for by the use of a higher sampling rate (Van Vleck & Middleton 1966; Burns & Yao 1969; Thompson et al. 2001), the 1 bit quantization does not have an effect on the parameters of a pulsar-like period, DM, etc. (see Table 2). Most of the modern low-frequency radio telescopes have multibit digital receivers that provide a higher dynamic range (Taylor et al. 2012; van Haarlem et al. 2013; Prabu et al. 2015; Reddy et al. 2017; Zarka et al. 2020; Girish et al. 2023). However, in a relatively minimal RFI location like Gauribidanur (Monstein et al. 2007; Kishore et al. 2015; Hariharan et al. 2016b; Bane et al. 2024), a lower dynamic range digital receiver can be used (see e.g., Zakharenko et al. 2016). Our results indicate that in such circumstances the sensitivity to observe faint events within a short time interval depends largely on the effective collecting area and the observing bandwidth. It is well known that absolute flux measurements can be difficult in 1 bit receivers (Van Vleck & Middleton 1966; Udaya Shankar & Ravi Shankar 1990; Ramkumar et al. 1994; Ramesh et al. 2006; Stein 2019). But in a wide-field multibeam system where the primary requirement is to cover the maximum area of the sky with high temporal and spectral resolution, such binary receiver systems can be beneficial. Overall, the 1 bit receiver offers flexibility, allowing for multiple simultaneous beams in different directions, different integration times and frequency channel widths, and different filtering algorithms to be used. Further, the archival data can be stored in raw form with fewer resources and reprocessed in the future as per requirements. Reports indicate that 1 bit raw voltage recording has also been used at higher frequencies (Teng et al. 2015). With the

currently available technology, sampling rates up to ≈ 40 GHz can be achieved.

Acknowledgments

We are grateful to the Gauribidanur Observatory team for their help in the observations and upkeep of the facilities. A. A. Deshpande is thanked for his encouragement and suggestions. We acknowledge the referee for the kind comments, which helped to present the results more clearly.

ORCID iDs

Kshitij S. Bane  <https://orcid.org/0000-0002-8550-9070>
G. V. S. Gireesh  <https://orcid.org/0000-0003-0741-0144>
C. Kathiravan  <https://orcid.org/0000-0002-6126-8962>
R. Ramesh  <https://orcid.org/0000-0003-2651-0204>

References

- Bane, K. S., Barve, I. V., Gireesh, G. V. S., Kathiravan, C., & Ramesh, R. 2022, *JATIS*, **8**, 017001
- Bane, K. S., Barve, I. V., Gireesh, G. V. S., Kathiravan, C., & Ramesh, R. 2024, *JATIS*, **10**, 014001
- Benz, A. O., Monstein, C., Meyer, H., et al. 2009, *EM&P*, **104**, 277
- Bilous, A. V., Bondonneau, L., Kondratiev, V. I., et al. 2020, *A&A*, **635**, A75
- Bondonneau, L., Griefmeier, J.-M., Theureau, G., et al. 2020, *A&A*, **635**, A76
- Burns, W. R., & Yao, S. S. 1969, *RaSc*, **4**, 431
- Ebenezer, E., Ramesh, R., Subramanian, K. R., Sundara Rajan, M. S., & Sastry, C. V. 2001, *A&A*, **367**, 1112
- Girish, B. S., Reddy, S. H., Sethi, S., et al. 2023, *JApA*, **44**, 28
- Hariharan, K., Ramesh, R., Kathiravan, C., Abhilash, H. N., & Rajalingam, M. 2016b, *ApJS*, **222**, 21
- Hassall, T. E., Stappers, B. W., Hessels, J. W. T., et al. 2012, *A&A*, **543**, A66
- Kishore, P., Kathiravan, C., Ramesh, R., Rajalingam, M., & Indrajit, V. B. 2014, *SoPh*, **289**, 3995
- Kishore, P., Ramesh, R., Kathiravan, C., & Rajalingam, M. 2015, *SoPh*, **290**, 2409
- Landecker, T. L. 1984, *ITIM*, **33**, 78
- Maan, Y., van Leeuwen, J., & Vohl, D. 2021, *A&A*, **650**, A80
- Malov, O. I., & Malofeev, V. M. 2010, *ARep*, **54**, 210
- McLean, D. J., & Labrum, N. R. 1985, *Solar Radio Physics: Studies of Emission from the Sun at Meter Wavelengths* (Cambridge: Cambridge Univ. Press)
- Monstein, C., Ramesh, R., & Kathiravan, C. 2007, *BASI*, **35**, 473
- Nakajima, H., Nishio, M., Enome, S., et al. 1994, *IEEEP*, **82**, 705
- Pilia, M., Hessels, J. W. T., Stappers, B. W., et al. 2016, *A&A*, **586**, A92
- Prabu, T., Srivani, K. S., Roshi, A. D., et al. 2015, *ExA*, **39**, 73
- Ramesh, R. 2011, *ASInC*, **2**, 55
- Ramesh, R., & Ebenezer, E. 2001, *ApJL*, **558**, L141

- Ramesh, R., Kathiravan, C., Indrajit, V. B., & Rajalingam, M. 2012, *ApJ*, **744**, 165
- Ramesh, R., Kathiravan, C., Sundara Rajan, M. S., Indrajit, V. B., & Sastry, C. V. 2008, *SoPh*, **253**, 319
- Ramesh, R., Kathiravan, C., Sundara Rajan, M. S., Indrajit, V. B., & Rajalingam, M. 2014, *ASInC*, **13**, 19
- Ramesh, R., Subramanian, K. R., & Sastry, C. V. 1999, *SoPh*, **185**, 77
- Ramesh, R., Subramanian, K. R., Sundara Rajan, M. S., & Sastry, C. V. 1998, *SoPh*, **181**, 439
- Ramesh, R., Sundara Rajan, M. S., & Sastry, C. V. 2006, *ExA*, **21**, 31
- Ramkumar, P. S., Prabu, T., Girimaji, M., & Markendeyalu, G. 1994, *JApA*, **15**, 343
- Ransom, S., 2011 PRESTO: Pulsar Exploration and Search TOolkit, Astrophysics Source Code Library, ascl:[1107.017](https://ui.adsabs.org/abs/1107.017)
- Reddy, S. H., Kudale, S., Gokhale, U., et al. 2017, *JAI*, **6**, 1641011
- Stein, M. S. 2019, arXiv:[1905.12528](https://arxiv.org/abs/1905.12528)
- Stovall, K., Ray, P. S., Blythe, J., et al. 2015, *ApJ*, **808**, 156
- Taylor, G. B., Ellingson, S. W., Kassim, N. E., et al. 2012, *JAI*, **1**, 1250004
- Teng, H. F., Zhang, U. H., Chiueh, T. H., et al. 2015, *ITIM*, **64**, 299
- Thompson, A. R., Moran, J. M., & Swenson, G. W., Jr 2001, *Interferometry and Synthesis in Radio Astronomy* (2nd ed.; New York: Wiley-Interscience)
- Udaya Shankar, N., & Ravi Shankar, T. S. 1990, *JApA*, **11**, 297
- van Haarlem, M. P., Wise, M. W., Gunst, A. W., et al. 2013, *A&A*, **556**, A2
- Van Vleck, J. H., & Middleton, D. 1966, *IEEEP*, **54**, 2
- Weinreb, S. 1963, PhD thesis, Massachusetts Institute of Technology
- Zakharenko, V., Konavalenko, A. A., Zarka, P., et al. 2016, *JAI*, **5**, 1641010
- Zakharenko, V. V., Vasylieva, I. Y., Konovalenko, A. A., et al. 2013, *MNRAS*, **431**, 3624
- Zarka, P., Denis, L., Tagger, M., et al. 2020, 23rd URSI General Assembly and Scientific Symp. (International Union of Radio Science), <https://tinyurl.com/ycocd5ly>